Journal of Materials Chemistry A

Accepted Manuscript

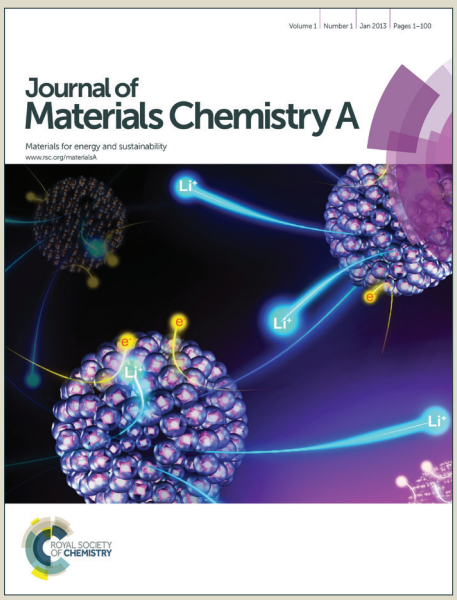

ROYAL SOCIETY OF CHEMISTRY

www.rsc.org/materialsA

Cite this: DOI: 10.1039/c0xx00000x

www.rsc.org/xxxxxx

ARTICLE TYPE

Graphene/Carbon-Coated Fe_3O_4 Nanoparticles Hybrids for Enhanced Lithium Storage†

Xin Jiang, Xiaoling Yang, Yihua Zhu,* Yifan Yao, Peng Zhao, Chunzhong Li*

Received (in XXX, XXX) XthXXXXXXXXX 20XX, Accepted Xth XXXXXXXXX 20XX

DOI: 10.1039/b000000x

A novel hierarchical nanostructure composed of carbon coated Fe_3O_4 nanoparticles with seed-like morphology distributing on graphene (denoted as G/Fe_3O_4@C) is prepared as a high-capacity anode electrode for LIBs. β-FeOOH nanoseeds were firstly assembled on graphene by solvothermal treatment, followed by coating β-FeOOH nanoseeds with polydopamine *via* immersion in dopamine aqueous solution. Finally, G/Fe_3O_4@C is obtained after *in situ* phase transformation of β-FeOOH to Fe_3O_4 and simultaneously carbonization of polydopamine nanocoating through a thermal annealing at 500 °C. The thickness of the uniform and continuous carbon layer can be easily tailored by varying the polymerization time and the concentration of dopamine to balance the concurrent needs for high active material content and structure stability. The carbon layer can effectively prevent the agglomeration of Fe_3O_4 nanoparticles, which enables the reversible conversion reaction between Fe_3O_4 and lithium, and significantly improves the mechanic stability of electrodes by accommodating volume expansion of Fe_3O_4 nanoparticles during the electrochemical cycling. Meanwhile, the combination of graphene and carbon shell improves the electrochemical reaction kinetics of electrode. As a result, the obtained G/Fe_3O_4@C nanocomposites with the optimal carbon shell thickness of about 1.2 nm exhibit high reversible capacities with remarkable cyclic retention at different current rates (1344 mA h g^{-1} after cycling at 0.5 C for 200 cycles, 743 mA h g^{-1} after further cycling at 2 C for another 200 cycles) and excellent rate performance (150 mA h g^{-1} at 20 C) as anodes in lithium ion batteries.

1 Introduction

To achieve the next generation of rechargeable lithium-ion batteries (LIBs) with improved energy and power density, and excellent cyclic stability for further applications in hybrid electric vehicles (HEVs) and electric vehicles (EVs), considerable efforts have been made recently in developing new electrode materials or designing novel nanostructures. Nowadays, electrode compounds reacting through conversion reactions, such as transition metal oxides (Fe_3O_4,[1] Fe_2O_3,[2] and Co_3O_4[3]), are capable of Li^+ insertion/extraction in excess of 6 Li^+ per formula unit, resulting in a significantly larger reversible capacity (~ 700-1000 mA h g^{-1}) than that of traditional graphite anode (372 mA h g^{-1}).[4] However, the severe volume change occurs for this category of materials during lithium ion insertion/extraction, leading to structural disintegration and poor cycling performance, which are main drawbacks for commercial development.[5, 6] It is an effective approach for tackling the above obstacles to combine conversion-based electrodes with conductive materials and/or wrapped with high conductive materials.[7] Graphene, a 2-dimensional nanostructure of carbon atoms arranged in a honeycomb lattice, is the most popular "matrix" material to be composited with high-capacity metal oxides, due to its superior electrical conductivity, high surface area, and chemical stability.[8, 9] These intriguing merits make graphene in composites not only cushions the internal stress induced during the volume change but also serves as conductive paths for fast transfer of electrons.

On the other hand, differing from classical lithium insertion-extraction or lithium alloying processes, conversion reaction mechanism involves the formation and decomposition of Li_2O, which accompanies the reduction and oxidation of metal oxides (as shown in the following equation 1).[10, 11]

$M_xO_y + 2yLi^+ + 2ye^- \leftrightarrow yLi_2O + xM$ (M = Fe, Co, Ni, Cu, etc.) (1)

The reversible electrochemical lithium storage proceeds more easily with the nanoscale electrode, due to the fact that the extraction of lithium from bulk Li_2O is thermodynamically unfavorable.[12, 13] Therefore, synthesis of stable nanosized metal oxides has become very important for their high electrochemical performance. Fe_3O_4-based nanostructured materials (including nanoparticles,[14] nanocubes,[15] nanorods,[16] nanotubes,[17] nanodisks,[18] etc.) are attracting growing attention as high-capacity anode electrodes for LIBs due to their high theoretical capacity (928 mA h g^{-1}), low cost, eco-friendliness, and the natural abundance of iron.[19] Nanostructure provides a very short lithium ion diffusion length (L) within electrochemically active particle, thus significantly reducing the characteristic time constant (t) for ion diffusion, which makes it possible for nanostructured Fe_3O_4 materials to achieve an excellent rate

capability.[20] Furthermore, in order to integrate both the optimized electrochemical reaction and electrical conductivity, efforts have been put in combining nanostructured Fe_3O_4 and graphene matrix for high capacity and high power LIB anodes.

Nevertheless, the exposed Fe_3O_4 nanostructures on the graphene surface are still prone to aggregate during the electrochemical cycling, thus the cracking and pulverization of the electrodes are difficult to avoid, which leads to a decreased electrochemical performance of graphene/Fe_3O_4 hybrids.[21, 22] Furthermore, in many nanostructured transition metal oxides, the SEI films formed during Li uptake might be catalyzed by transition metal upon Li extraction to disappear completely, leading to capacity fading and safety problems.[23-25] Wrapping nanostructures within highly conductive carbon shells on graphene to form a close structure can tackle the aggregation of nanomaterials and keep the overall electrode highly conductive while leading to stabilized SEI films.[7, 23] Su et al. fabricated 2D graphene@metal oxide nanosheets confined within a carbon layer (G@MO@C) and obtained an outstanding lithium storage performance.[26] The concept of 2D core-shell nanomaterials on the surface of graphene could be utilized to fabricate excellent conversion/alloy-style electrode materials. Herein, we report a novel hierarchical nanostructure composed of carbon coated Fe_3O_4 nanoparticles with seed-like morphology distributed on graphene (denoted as G/Fe_3O_4@C). β-FeOOH nanoseeds were firstly assembled on graphene by solvothermal treatment. Next, β-FeOOH nanoseeds were coated with polydopamine *via* immersion in dopamine aqueous solution. Finally, G/Fe_3O_4@C is obtained after in situ phase transformation of β-FeOOH and simultaneously carbonization of polydopamine nanocoating by a thermal annealing at 500 ° C. Benefited from the excellent electroconductive network, uniform distribution and nanosize of Fe_3O_4 particles, high contact surface area and the efficient protection of carbon shell, the resulting G/Fe_3O_4@C (1.0/6), in which 1.0 and 6 represented the initial concentration of dopamine (1.0 mg mL^{-1}) and the polymerization time (h), respectively, delivered outstanding cycling performance as high as 1344 mA h g^{-1} (after cycling at 0.5 C for 200 cycles) and 743 mA h g^{-1} (after further cycling at 2 C for another 200 cycles), and good rate capacity up to 150 mA h g^{-1} (20 C) when evaluated as an anode material for LIBs.

2 Experimental

2.1 Reagents and materials

Graphite powder, Iron (III) chloride hexahydrate ($FeCl_3 \cdot 6H_2O$), Cetyltrimethylammonium bromide (CTAB), and ethanol were purchased from Sinopharm Chemical Reagent Co., Ltd. Sodium hydroxide (NaOH) was purchased from Shang-hai Lingfeng Chemical Reagent Co., Ltd. All the chemicals were of analytical grade and used as received. Deionized water was used in all experiments.

2.2 Preparation of G/β-FeOOH

Firstly, graphene/β-FeOOH nanoseeds nanocomposites were fabricated by a facile solvothermal process. Graphite oxide was prepared from natural graphite flakes according to the modified Hummers method.[27] In a typical synthesis, 0.1 g of graphite oxide was first dispersed in mixed solvent of ethanol and water (42 mL, volume ratio 5:1) by sonication for 1.5 h to form a homogeneous dispersion. Subsequently, CTAB (0.8 g) was added into the mixture with vigorous stirring for uniform dispersion before the addition of the proper amount of acid to adjust the pH value to about 2.0, as part A. 0.8 g of $FeCl_3 \cdot 6H_2O$ was dissolved into 2 mL of ethanol. After being stirred for 0.5 h, 1 mL of deionized water was added dropwise, then 1 mL of NaOH solution (16 mg mL^{-1}) was also added into the mixture, which was kept stirring for 15 min. The resulting mixture was filtered with a PTFE membrane with 1 μm pore size. The filtered solution, as part B, was then mixed with part A under vigorous stirring. The final suspended solution was transferred into a 100 mL Teflon-lined stainless steel autoclave and solvothermally treated at 120 °C for 14 h. The graphene/β-FeOOH nanocomposites were collected by centrifugation, washed thoroughly with warm ethanol and water and then dried at 60 °C in a vacuum box overnight.

2.3 Preparation of G/Fe_3O_4@C

200 mg of graphene/β-FeOOH was dispersed in 50 mL Tris-buffer (pH: ~8.5) by ultrasonication for 30 min to form a suspension. Subsequently, 50 mg dopamine was added to the mixture under stirring. The mixture was subjected to continuous magnetic stirring at 30 ° C for 6 h. Afterwards, the precipitates (graphene/β-FeOOH@polydopamine) were collected by centrifugation, washed thoroughly with deionized water and then dried at 60 ° C in a vacuum box overnight. The resulting sample was heated in a quartz tube to 150 °C at a rate of 3 °C min^{-1} in Ar atmosphere and kept at this temperature for 1 h, and then further heated to 500 °C with a heating rate of 5 °C min^{-1}, and kept at this temperature for 6 h. The obtained composite was denoted as G/Fe_3O_4@C (1.0/6), in which 1.0 and 6 represented the initial concentration of dopamine (1.0 mg mL^{-1}) and the polymerization time (h), respectively.

In order to tune the coating thickness of the carbon layer, samples were prepared by varying the polymerization time and the concentration of dopamine, labeled as G/Fe_3O_4@C (1.0/4) and G/Fe_3O_4@C (1.5/6). Meanwhile, G/Fe_3O_4 without carbon shell was also prepared in a similar process in the absence of dopamine.

2.4 Structure and morphology characterization

Powder X-ray diffraction (XRD) measurements were carried out by a polycrystalline X-ray diffractometer (RIGAKU, D/MAX 2550 VB/PC, λ = 1.5406 Å). Fouriertrans form infrared (FTIR) and Raman spectra were recorded on a Nicolet 5700 FTIR spectrometer and a Renishaw inVia Raman microprobe with excitation laser beam wavelength of 514 nm, respectively. The thermogravimetric (TG) measurement was carried out using a Mettler STARe thermal analyzer under a flow of air with a temperature ramp of 10 °C min^{-1} from room temperature to 800 °C. A JEOL SM-6360LV microscope (SEM), equipped with an energy dispersive X-ray analyzer (EDX), was used to investigate themorphologies and chemical compositions of the samples. The transmission electron microscopy (TEM) and selected area electron diffraction (SAED) was conducted on a JEM-2100 microscope operated at 200 kV.

2.5 Electrochemical measurements

All the electrochemical studies were conducted in two-electrode

coin-cell (CR 2016) assembled in an argon-filled glovebox. The working electrode composed of 80 wt% active material, 10 wt% poly(vinylidene fluoride) (PVDF), and 10 wt% carbon black was fabricated by casting a slurry onto a copper foil, and then dried in a vacuum oven at 80 °C for 12 h. The loading density of active material is 0.5 mg cm^{-2} and coating thickness is 14 μm. Metallic Li sheets were used both as counter and reference electrodes and a polypropylene film (Celgard 2400) was used as a separator. The nonaqueous electrolyte used was a 1.0 M $LiPF_6$ in EC/DMC (1:1 wt/wt). Galvanostatical charge-discharge cycles were carried out on a LAND-CT2001A battery tester at various current densities in the voltage range of 0.01-3.0 V versus Li^+/Li. Cyclic voltammetry and electrochemical impedance spectroscopy (EIS) measurements were carried out on an electrochemical workstation (Autolab PGSTAT30 potentiostat). The cyclic voltammograms were obtained over the potential range from 3.0 to 0.01 V at a scanning rate of 0.5 mV s^{-1}. The impedance spectra were obtained by applying an AC voltage of 5 mV amplitude over the frequency range from 100 kHz to 0.01 Hz at delithiation states.

3 Results and discussion

The overall synthetic procedure of $G/Fe_3O_4@C$ was illustrated in Fig. 1. It is well known that single layer of GO in solution was negatively charged. Thus, after CTAB was added in the stirring GO solution, the CTA^+ ions attached randomly on the surface of GO through electrostatic interactions.[28, 29] Subsequently, Fe^{3+} ions existing in filtered solution were added into the GO-CTA^+ solution and some of those were absorbed in the outward end of the micelles because of the electrostatic effects, while the others were still dispersed in the solution.[30] When the redox reaction was carried out in the acidic solvothermal system, FeOOH nanowires formed and then FeOOH nanowires dispersed in the solution self-assembled parallelly to those lying on GO to form nanorods.[30, 31] Finally, the FeOOH nanorods were epitaxial fused together to form β-FeOOH nanoseeds.[31] Meanwhile, GO could be well reduced to graphene under the solvothermal condition, thus obtained G/β-FeOOH nanoseeds nanocomposites. Afterwards, β-FeOOH were coated with polydopamine though the bind between the surface -OH of β-FeOOH and the catechol-derivative anchor groups of dopamine, after immersion of G/β-FeOOH in dopamine aqueous solution.[32] Subsequently, through a thermal annealing at 500 °C, G/β-FeOOH@polydopamine was successfully transformed into $G/Fe_3O_4@C$ nanocomposites.[33]

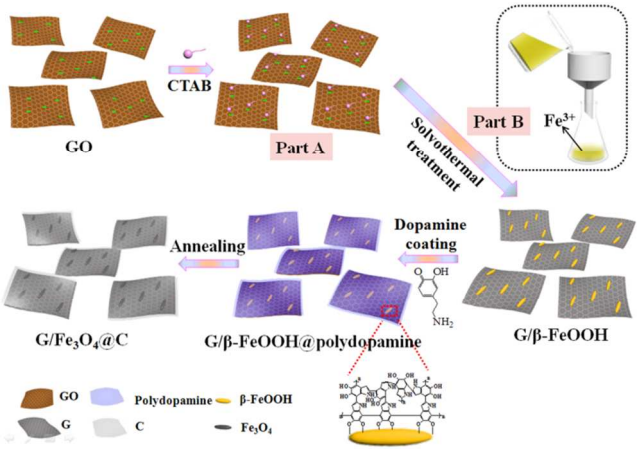

Fig. 1 Schematic illustration for fabricating $G/Fe_3O_4@C$.

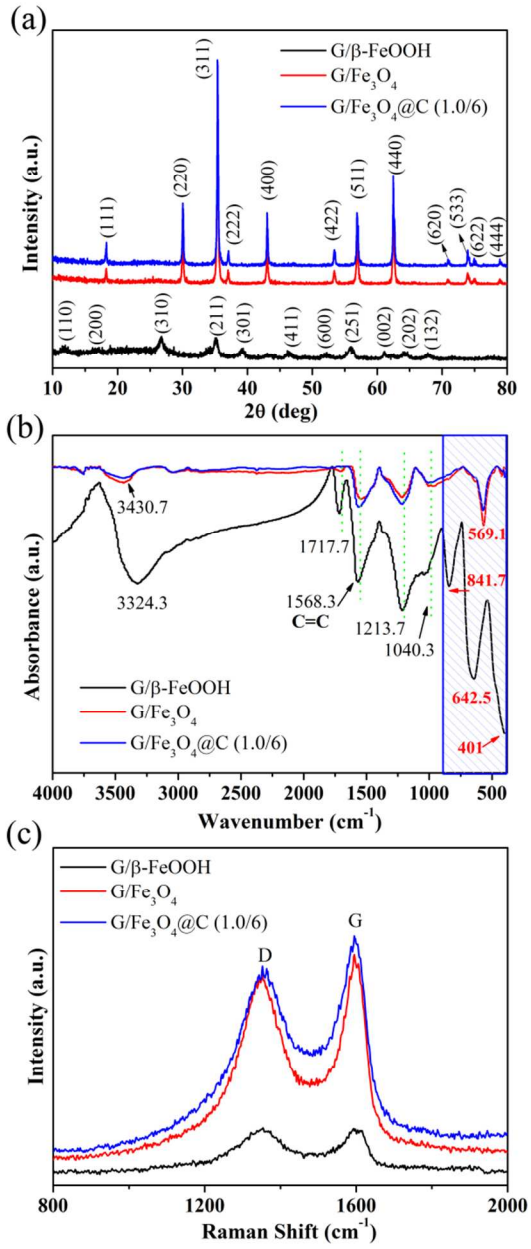

Fig. 2 (a) XRD patterns, (b) FTIR spectra, and (c) Raman spectra of G/β-FeOOH, G/Fe_3O_4 without carbon shell, and $G/Fe_3O_4@C$ (1.0/6), respectively.

A powder X-ray diffraction (XRD) experiment was carried out to gain insight into the internal structure of G/β-FeOOH, G/Fe_3O_4 and $G/Fe_3O_4@C$ (1.0/6). As shown in Fig. 2a, the distinct diffraction pattern of solvothermally treated product was in good agreement with β-FeOOH (JCPDS No. 75-1594). In contrast, both products (G/Fe_3O_4 and $G/Fe_3O_4@C$ (1.0/6)) after annealing process exhibited similar patterns, and all intensive peaks can be well indexed to pure Fe_3O_4 (JCPDS No.85-1436), suggesting that the akagenite particles had been transformed into the face-centered cubic phase of magnetite after the pyrolysis. The XRD pattern of $G/Fe_3O_4@C$ (1.0/6) lacked peaks corresponding to graphite, indicating that the carbon layer was amorphous.[19] Further insights of the structural and compositional properties of

composites were obtained from Flourier transform infrared spectroscopy (FTIR) spectra (Fig. 2b). Characteristic peaks of β-FeOOH (at around 401 cm^{-1} corresponding to Fe-O stretching vibration, and at 642.5 and 841.7 cm^{-1} corresponding to the deformation mode of Fe-OH groups) were found in the curve of G/β-FeOOH sample,[34, 35] and these peaks disappeared and a new preak at 569.1 cm^{-1} corresponding to the stretching vibration of the Fe-O bond of Fe_3O_4 arisen in the curves of G/Fe_3O_4 and G/Fe_3O_4@C (1.0/6). Meanwhile, the characteristic peaks of oxygen-containing functional groups, including 3430.7 cm^{-1} for O-H stretching, 1717.7 cm^{-1} for C=O stretching of COOH groups, 1213.7 cm^{-1} for phenolic C-OH stretching, and 1040.3 cm^{-1} for C-O stretching, were decreased dramatically in intensity after the annealing process, implying that rGO obtained after solvothermal reduction was further reduced to graphene. As a result, the electrical conductivity could be improved, which was favorable for the efficient energy storage.[36] Raman spectra of three samples (Fig. 2c) displayed two prominent peaks at ~1349 cm^{-1} (D band originating from defects associated with vacancies, grain boundaries, and amorphous carbon species) and 1595 cm^{-1} (G band corresponding to ordered sp^2-bonded carbon atoms), respectively.[37] The intensity ratios of D band to G band for G/Fe_3O_4 and G/Fe_3O_4@C (1.0-6h) showed decreased values compared with that for G/β-FeOOH, indicating the further recovered aromatic structures after the removal of oxygen moieties by thermal reduction,[38] consistent with the result of FTIR spectra.

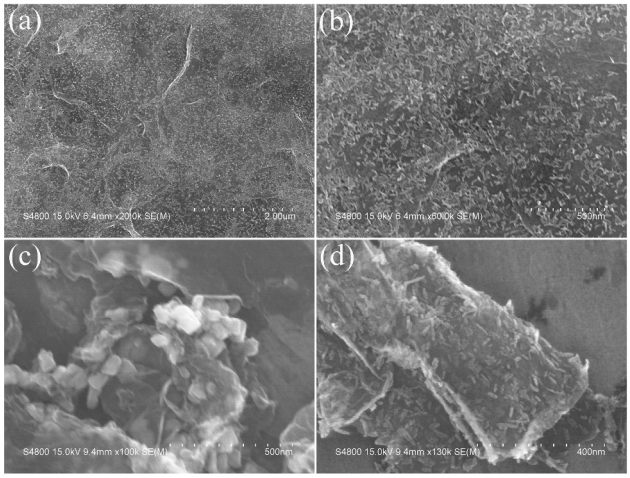

Fig. 3 (a) Low-magnification and (b) high-magnification SEM images of the G/β-FeOOH. The SEM images of (c) G/Fe_3O_4 without carbon shell and (d) G/Fe_3O_4@C (1.0/6).

The morphology and structure of the products were characterized by SEM images (Fig. 3). As shown in Fig. 3a and 3b, plenty of β-FeOOH nanoparticles with seed-like morphology were uniformly anchored on the wrinkling graphene surface, suggesting efficient assembly between β-FeOOH nanoparticles and graphene sheets during the solvothermal treatment. These seed-shaped nanoparticles exhibited a homogenous particle size with diameters of about 10 nm and lengths of 20-40 nm. Interestingly, when mixed solution (part B) wasn't filtered with a PTFE membrane with 1 μm pore size, while keeping the other experimental variables fixed, we obtained β-FeOOH nanospindles besides of nanoseeds (Fig. S1a and 1b). It was more likely because that the high Fe^{3+} concentration caused the growth of crystal. Further, when CTAB was also not used, only β-FeOOH nanospindles were obtained, as shown in Fig. S1c, which was ascribed to that CTAB could confine the growth of particles in the nanometer regime.[39] After phase transformation of β-FeOOH to Fe_3O_4 through a thermal annealing at 500 °C, the seed-like morphology in G/Fe_3O_4 without carbon shell turned into irregular and larger particle size was observed, as shown in Fig. 3c. Whereas, there was no significant change in overall hierarchical nanostructure of G/Fe_3O_4@C (1.0/6), as shown in Fig. 3d, which might be because the uniform carbon shell could effectively prevent the adjacent nanoparticles from coalescing and maintain the shape of particles during the thermal treatment. Fig. S2 showed the corresponding energy dispersive X-ray spectrum (EDS) of G/Fe_3O_4 and G/Fe_3O_4@C (1.0/6). Carbon content estimated from EDS analysis were found to be 25.1 wt% and 38.19 wt% for G/Fe_3O_4 and G/Fe_3O_4@C (1.0/6), respectively.

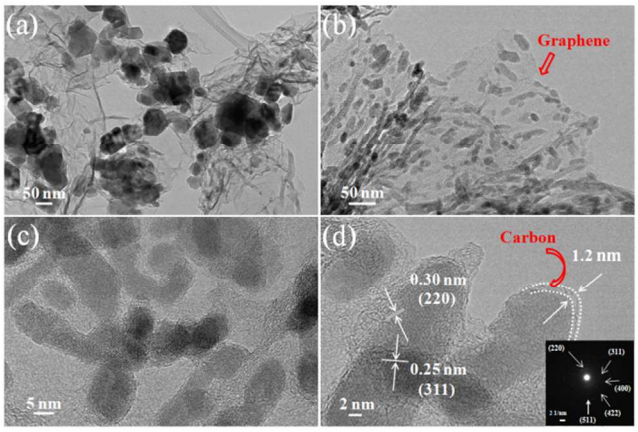

Fig. 4 (a) TEM image of G/Fe_3O_4. (b) TEM and (c and d) HRTEM images of G/Fe_3O_4@C (1.0/6). (Inset in 4d) the SAED pattern of G/Fe_3O_4@C (1.0/6).

The microstructures of G/Fe_3O_4 and G/Fe_3O_4@C (1.0/6) were further examined using transmission electron microscopy (TEM) and were presented in Fig. 4. As shown in Fig. 4a, Fe_3O_4 nanoparticles in G/Fe_3O_4 with size of about 50 nm showed serious aggregation, which could inhibit the Li-ion diffusion and electrolyte access. In contrast, Fe_3O_4 in G/Fe_3O_4@C (1.0/6) featuring diameters of about 7 nm and lengths of about 20 nm still uniformly distributed on graphene with few aggregations due to the confinement of carbon shell (In Fig. 4b and 4c), thus making them fully accessible to lithium ions in the electrolyte. The slightly reduced size of Fe_3O_4 nanoseeds compared to that of initial β-FeOOH nanoseeds was ascribed to the volume contraction associated with the transformation from low density β-FeOOH (3 g cm^{-3}) to denser magnetite with a density of 5.18 g cm^{-3} after the annealing process.[40] In Fig. 4d, the HRTEM image of G/Fe_3O_4@C (1.0/6) shown that the entire surface of Fe_3O_4 nanoseeds had been covered with a uniform and continuous amorphous carbon shell with the thickness of about 1.2 nm to form a close composite structure. Such a geometric confinement effectively suppressed the dissolution and agglomeration of nanoseeds during the cycling, thereby promoting the electrochemical activity and stability of the nanocomposites.[41] Besides, amorphous carbon could allow Li ions to pass through

carbon layer to react with inner Fe_3O_4 nanoseeds as compared to crystallized carbon.[42] The visible set of lattice fringes with *d*-spacing of 0.30 and 0.25 nm corresponded to (220) and (331) lattice planes of Fe_3O_4, respectively. The corresponding SAED pattern (Inset in Fig. 4d) showed multiple concentric circles, which can be indexed to the (220), (311), (400), (422), and (511) lattice planes, confirming the polycrystalline nature of Fe_3O_4. Energy-dispersive X-ray spectroscopy elemental mapping was used to help understand the distribution and composition of G/Fe_3O_4@C (1.0/6). As shown in Fig. 5, the concordance of C, Fe and O signals confirmed that Fe_3O_4 particles were homogeneously distributed in the composite. Moreover, the evenly distributed points of N element, which doped in carbon derived from polydopamine after pyrolysis,[43] further confirmed the homogeneous carbon shell cover on the nanocomposite.

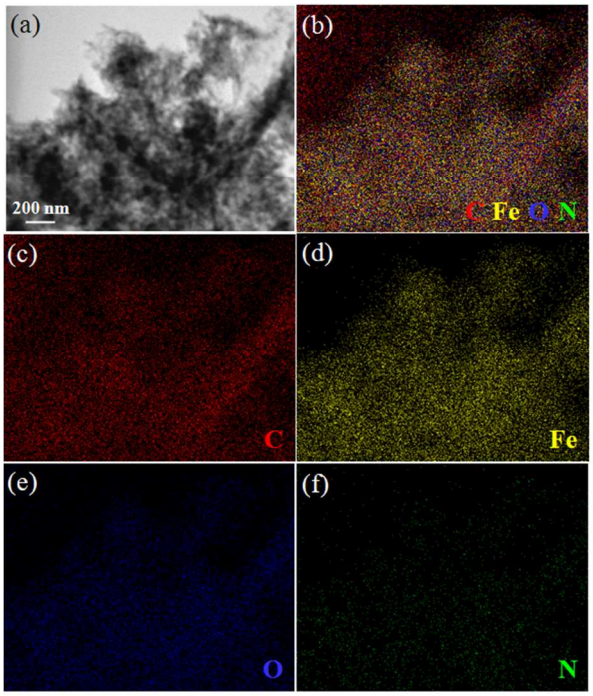

Fig. 5 (a) Scanning transmission electron microscopy (STEM) image of G/Fe_3O_4@C (1.0/6), and (b-f) the corresponding EDX mapping images of carbon, iron, oxygen, nitrogen elements.

In order to determine the optimal composition for electrochemical performance, G/Fe_3O_4@C nanocomposites with different carbon thickness were also prepared by simply adjusting the polymerization time and the concentrations of initial dopamine, while keeping the other experimental variables fixed. The polymerization time was shorted from 6 to 4 h or initial dopamine concentration was varied from 1.0 to 1.5 mg mL^{-1}, and the corresponding products were named G/Fe_3O_4@C (1.0/4) and G/Fe_3O_4@C (1.5/6), respectively. As seen from the TEM images (Fig. 6a and 6b), the carbon shell in G/Fe_3O_4@C (1.0/4) and G/Fe_3O_4@C (1.5/6) was about 0.6 and 4.3 nm in thickness, respectively. However, it should be noticed that uncontinuous carbon shell and serious aggregation of partial particles with random shape were observed in G/Fe_3O_4@C (1.0/4), possibly because of the relatively low dopamine concentration and limited polymerization time (Fig. S3). Thermogravimetric (TG) analysis was used to determine chemical composition of products as shown in Fig. 6c. From the images we could see that as the polymerization time or the initial concentration increased, the weight loss of the corresponding product was greater. The content of carbon was 23.5 wt%, 28.7wt%, 30.8 wt% and 40.0 wt% for products G/Fe_3O_4, G/Fe_3O_4@C (1.0/4), G/Fe_3O_4@C (1.0/6), and G/Fe_3O_4@C (1.5/6), respectively, which matched well with the result of element analysis for G/Fe_3O_4 and G/Fe_3O_4@C (1.0/6). The TG curves of Fe_3O_4 and graphene were showed in Fig. S4.

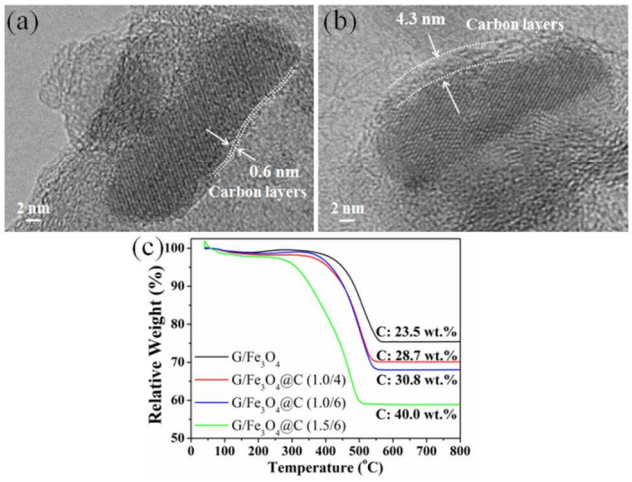

Fig. 6 TEM image of (a) G/Fe_3O_4@C (1.0/4) and (b) G/Fe_3O_4@C (1.5/6). (c) TG curves of G/Fe_3O_4@C nanocomposites with different carbon content.

The integration of crystalline nanoparticles, uniform carbon coating as well as graphene conducting network should lead to improvement in conducting properties and structure integrity, and therefore the overall electrochemical reversibility for Li^+ storage. In order to characterize electrochemical properties of these products, coin cells with the lithium foil as the counter electrode were fabricated. The charge storage behavior was first characterized by cyclic voltammetry (CV) scanned at a rate of 0.5 mV s^{-1} between 0.01 and 3.0 V. In the cathodic curve of the first cycle, both G/Fe_3O_4 nanocomposites and G/Fe_3O_4@C (1.0/6) nanocomposites exhibited two well-defined peaks, as shown in Fig. 7a and 7b. The peak at 1.41 V for G/Fe_3O_4 and 1.43 V for G/Fe_3O_4@C (1.0/6) corresponded to the structure transition induced by lithium intercalation into crystalline Fe_3O_4 (Fe_3O_4 + xLi^+ + xe^- → $Li_xFe_3O_4$). The main peak at 0.42 V for G/Fe_3O_4 and 0.47 V for G/Fe_3O_4@C (1.0/6) was attributed to the further reduction of $Li_xFe_3O_4$ to Fe and the formation of amorphous Li_2O by conversion reaction [$Li_xFe_3O_4$ + (8 – x)Li^+ + (8 – x)e^- → 4Li_2O + 3Fe].[44] Note that the two main peaks shifted to higher voltage in the subsequent cycles due to the structure change in the Fe_3O_4 nanoparticles after the Li-ion insertion in the first cycle.[45] Meanwhile, in the anodic sweep, the wide peak at about 1.77 V for G/Fe_3O_4 and 1.89 V for G/Fe_3O_4@C (1.0/6) was ascribed to the oxidation of Fe^0 to Fe^{2+} and Fe^{3+} (3Fe + 4Li_2O → Fe_3O_4 + 8Li^+ + 8e^-). The slightly peak shift from 1.77 V for G/Fe_3O_4 to 1.89 V for G/Fe_3O_4@C (1.0/6) may be ascribed to the more oxidation of Fe^0 to Fe^{3+}, due to the structural change composed of the nanosized Fe_3O_4 particles, less aggregation, and higher carbon content, after adding the carbon shell.[46-48] It was noteworthy that, after the first cycle, there was no noticeable change of peak intensity and integrated areas for both

cathodic and anodic peaks of $G/Fe_3O_4@C$ (1.0/6) nanocomposites, which indicated that a stable SEI film formed on the surfaces and interfaces of nanocomposites, thus safeguarding the structural integrity of encapsulated Fe_3O_4 during subsequent charge-discharge cycles, leading to the stable and superior reversibility of the sample.[49] Fig. 7c and 7d presented the voltage profiles of G/Fe_3O_4 and $G/Fe_3O_4@C$ (1.0/6) nanocomposites charged and discharged at a current density of 93 mA g^{-1} (0.1 C) between 0.01 and 3.0 V versus Li/Li^+ for the first two cycles, respectively. The first discharge curves of two products were very similar, with one clear potential plateau at about 0.8 V versus Li^+/Li due to the reduction of Fe^{3+} to Fe^0, followed by a sloping curve down to the cutoff voltage of 0.01 V, which was close to that described in the literature for Fe_3O_4 anodes.[23] In agreement with the CV curves, the discharge curves of G/Fe_3O_4 and $G/Fe_3O_4@C$ (1.0/6) nanocomposites were different in the second cycle due to the drastic structural changes in the electrode. The initial lithiation and delithiation capacities of G/Fe_3O_4 were 2123 and 1302 mA h g^{-1}, respectively, with a Coulombic efficiency of 61.3 % (Fig. 7c). The initial capacity loss might result from the incomplete conversion reaction and irreversible lithium loss due to the formation of a solid electrolyte interphase (SEI) layer.[50] The reversible capacity was higher than the theoretical capacity of Fe_3O_4 (about 930 mA h g^{-1}), which was likely due to the formation of a pseudo-capacitive gel-like film resulting from the electrolyte decomposition at low voltages and larger electrochemical active surface area of graphene and/or grain boundary area of the nanosized Fe_3O_4 particles.[51, 52] The initial lithiation and delithiation capacities of $G/Fe_3O_4@C$ (1.0/6) decreased to 1568 and 1033 mAh g^{-1}, respectively, after carbon coating, whereas Coulombic efficiency increased to 65.9 %. Similar effects of carbon coating were obtained in reported literature,[12, 26] owing to that the amount of SEI was reduced by the carbon and less side reactions taking place since the contact area between Fe_3O_4 and electrolytes was reduced by blocking liquid electrolyte penetration into Fe_3O_4 nanoparticles.[53] In the second discharge-charge cycle, the $G/Fe_3O_4@C$ (1.0/6) nanocomposites exhibited a high reversible capacity of 1102 mA h g^{-1} and the corresponding Coulombic efficiency quickly rose to 92.4 %.

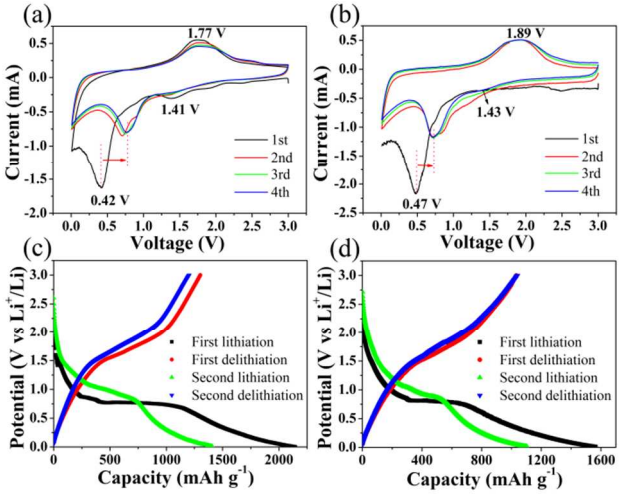

Fig. 7 Cyclic voltammograms of (a) G/Fe_3O_4 and (b) $G/Fe_3O_4@C$ (1.0/6) electrode between 0.01 and 3.0 V at a scan rate of 0.5 mV s^{-1} for the first four cycles, respectively. Charge-discharge curves of (c) G/Fe_3O_4 and (d) $G/Fe_3O_4@C$ (1.0/6) electrode in the first two cycles at a current density of 0.1 C (1 C = 930 mA g^{-1}).

Cyclic stability of G/Fe_3O_4, $G/Fe_3O_4@C$ (1.0/4), $G/Fe_3O_4@C$ (1.0/6), and $G/Fe_3O_4@C$ (1.5/6) was evaluated at a current density of 93 mA g^{-1} (0.1 C) for the first two cycles, followed by cycling at 465 mA g^{-1} (0.5 C) for 200 cycles, and then further at 1860 mA g^{-1} (2 C) for the last 200 cycles between 0.01 and 3.0 V versus Li/Li^+, as presented in Fig. 8a. The capacities of all samples showed an increasing trend at the beginning when cycling at 0.5 C, and this phenomenon was not uncommon for various nanostructured metal oxide electrodes, which could be ascribed to the organic polymeric/gel-like layer around the active materials to deliver excess capacity at low potential through a so-called "pseudo-capacitance-type behavior", and the activation of active materials to obtain more reaction sites.[54] However, after a gradual capacity increasing up to 1311 mA h g^{-1} about 90 cycles, G/Fe_3O_4 electrode then suffered from serious capacity fading, leading to a low capacity of 857 mA h g^{-1} after 202 cycles with a Coulombic efficiency of 98.4 % (Fig. 8b). In contrast, the capacity of $G/Fe_3O_4@C$ (1.0/6) electrode increased continuously to 1344 mA h g^{-1} after 202 cycles with a Coulombic efficiency of 99.1 %. It indicated a significantly improved cyclic stability resulting from the external carbon layer. The electrode based on $G/Fe_3O_4@C$ (1.0/4) also showed the gradual capacity fading after 101 cycles, and a reversible capacity of about 830 mA h g^{-1} after 202 cycles was obtained, similar to that of G/Fe_3O_4. This disappointing cycling performance could categorically be attributed to the large primary size of partial nanoparticles and inadequate carbon coating. $G/Fe_3O_4@C$ (1.5/6) with the highest carbon percentage, however, only delivered a charge capacity of 767 mA h g^{-1} at the end of 202 cycles due to the decrease in the proportion of electrochemically active component (Fe_3O_4).[33, 55] Hence the carbon content had to be optimized to balance the concurrent needs for high active material content and structure stability. Apparently, $G/Fe_3O_4@C$ (1.0/6) sample would be a candidate to achieve a balance between the specific capacity and cycle stability. For this sample, no obviously capacity decay was detected and a high reversible capacity of about 743 mA h g^{-1} with a Coulombic efficiency of 98.7 % was finally obtained, when further cycling at 2 C for another 200 cycles. The discharge-charge capacities of obtained electrodes were also measured at different C rates (Fig. 8c and Fig. S5). A total of 380 cycles were used, and the results indicated remarkable resilience in rate performance and capacity retention for $G/Fe_3O_4@C$ (1.0/6) electrode. It were initially cycled at 0.1 C where charge capacity was 1469 mA h g^{-1} in the first 20 cycles. The rate was then increased stepwise to 0.2, 0.5, 1, 2, 3, 5, 10, and 20 C in succession, and capacities of 1419, 1298, 1048, 757, 508, 405, 227, and 150 mA h g^{-1} stable for 40 discharge-charge cycles at each of these rates were obtained. When the C-rate was finally returned to its initial value of 0.1 C after 340 cycles, a charge capacity of 1447 mA h g^{-1} was still available. Other three electrodes showed weaker rate performance especially at high rate. This phenomenon could be attributed to uniform Fe_3O_4 particles with nanosize, enlarging the active material/electrolyte contact area and minimizing transport distances between the electrode and electrolyte, and the improved electronic

conductivity and ion permeability due to carbon coating with appropriate percentage.[33]

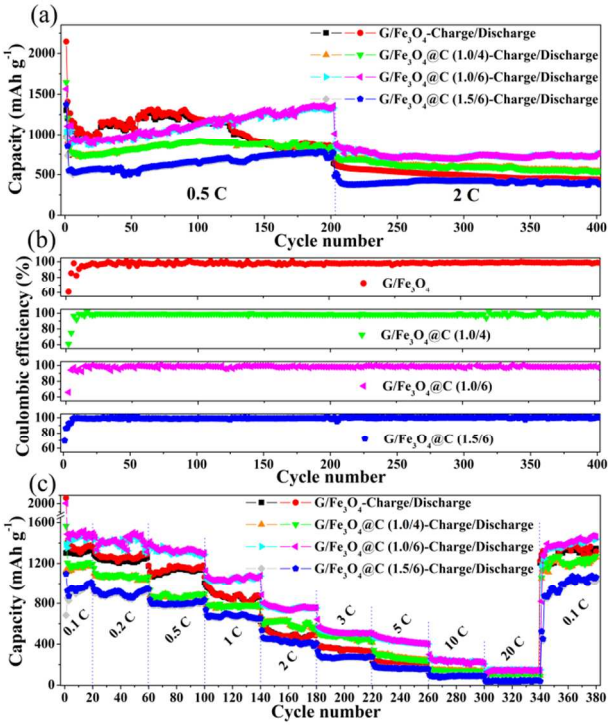

Fig. 8 (a) The comparative cycling performance of obtained electrodes: cycling at a current density of 93 mA g^{-1} (0.1 C) for the first two cycles, followed by cycling at 465 mA g^{-1} (0.5 C) for 200 cycles, then further at 1860 mA g^{-1} (2 C) for last 200 cycles. (b) The corresponding Coulombic efficiency. (c) Cycling performance of obtained electrodes at various current rates (0.1 C - 20 C).

The improved electrochemical performance of G/Fe_3O_4 after carbon coating could be ascribed to the following reasons: first, the presence of carbon shell was effective in preventing the aggregation of Fe_3O_4, which enabled the reversible conversion reaction between Fe_3O_4 and lithium to provide the high capacity, and significantly improving mechanic stability of electrode to enhance the cycle stability. The microstructures of cycled materials were investigated by TEM, as shown in Fig. 9a and 9b. Aggregation was significant for G/Fe_3O_4, and resulting in larger particle sizes (Fig. 9a). It made the extraction of lithium from Li_2O difficult, because the reverse reaction was thermodynamically favorable for nanosized materials,[13] which resulted in the fading lithium ion storage capacity upon extended cycling. For comparison, G/Fe_3O_4@C (1.0/6) were very stable and uniform Fe_3O_4 nanoparticles were well preserved after extended cycling (Fig. 9b), demonstrated that carbon nanocoating could effectively improve the structural stability by suppressing the aggregation of Fe_3O_4 nanoparticles and accommodating their volume expansion during the cycling. Second, stable nanosized Fe_3O_4 particles enlarged the electrode/electrolyte contact area and decreased electron and lithium ion diffusion distances significantly, thereby ensuring good rate capability. Additionally, the carbon shell of G/Fe_3O_4@C (1.0/6) could improve the conductivity of the electrode, thus introduce fast electron and ion transport, further improving the rate performance. These enhancements of the electrode kinetics could be shown more directly by electrochemical impedance spectroscopy (EIS) measurements. The G/Fe_3O_4 and G/Fe_3O_4@C (1.0/6) samples were analyzed by EIS at open-circuit voltages in their native states (before cycling), as shown in Fig. 9c. The equivalent circuit for the AC impedance spectra was depicted in Fig. S6. R_s and R_{ct} are the solution resistance and charge-transfer resistance, respectively. CPE is the double layer capacitance and passivation film capacitance. The value of the charge transfer resistance (R_{ct}) is 127 Ω for G/Fe_3O_4@C (1.0/6), which is significantly lower than that of G/Fe_3O_4 (314 Ω), indicating an overall smaller charge transfer resistance. All the above characteristics made G/Fe_3O_4@C (1.0/6) a promising anode material for high-performance LIBs.

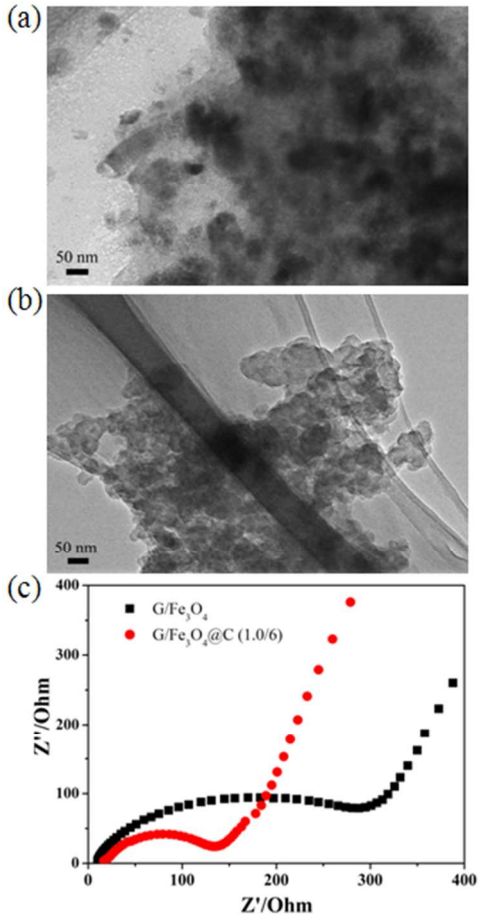

Fig. 9 TEM images of (a) G/Fe_3O and (b) G/Fe_3O_4@C (1.0/6) after 402 cycles at 0.1 C for the first two cycles and 0.5 C for the following 200 cycles and 2 C for the last 200 cycles between 0.01 and 3.0 V versus Li/Li^+. (c) Nyquist plots of G/Fe_3O_4 and G/Fe_3O_4@C (1.0/6) electrodes before cycling by applying an AC voltage of 5 mV amplitude over the frequency range from 100 kHz to 0.01 Hz.

4 Conclusions

In summary, we synthesized new carbon coated Fe_3O_4 nanoparticles with seed-like morphology on graphene by solvothermal reduction, subsequent simultaneously in situ phase transformation and modification with carbon nanocoating through a thermal annealing process. The thickness of the uniform and

continuous carbon layer could be easily tailored by varying the polymerization time and the concentration of dopamine, which allowed a balance between the specific capacities and cycling stability. Due to the efficient protection of the carbon shell, stable electrode structure and nanosized Fe_3O_4 particles with little aggregation were achieved, meanwhile, the combination of graphene and carbon shell improved the electrochemical reaction kinetics. As a result, the obtained G/Fe_3O_4@C (1.0/6) with the optimal carbon shell thickness exhibited superior electrochemical performance for LIBs.

Acknowledgements

This work was supported by the National Natural Science Foundation of China (21471056, 21236003, 21206042, and 21176083), the Basic Research Program of Shanghai (13NM1400700, 13NM1400701), and the Fundamental Research Funds for the Central Universities.

Notes and references

Key Laboratory for Ultrafine Materials of Ministry of Education, School of Materials Science and Engineering, East China University of Science and Technology, Shanghai 200237, China. Fax: +86 21 6425 0624; Tel: +86 21 6425 2022; E-mail: yhzhu@ecust.edu.cn and czli@ecust.edu.cn

†Electronic Supplementary Information (ESI) available*:* Detailed and additional Figure as noted in the text. See DOI: 10.1039/b000000x/

1 Y. Chen, B. H. Song, L.Lu and J. M. Xue, *Nanoscale*, 2013, **5**, 6797.
2 J. Miot, N. Recham, D. Larcher, F. Guyot, J. Brest and J. –M. Tarascon, *Energy Environ. Sci.*, 2014, **7**, 451.
3 X. L. Yang, K. C. Fan, Y. H. Zhu, J. H. Shen, X. Jiang, P. Zhao, S. R. Luan and C. Z. Li, *ACS Appl. Mater. Interfaces,* 2013, **5**, 997.
4 C. M. Ban, Z. C. Wu, D. T. Gillaspie, L. Chen, Y. F. Yan, J. L. Blackburn and A. C. Dillon, *Adv. Mater.*, 2010, **22**, E145.
5 K. Zhang, W. Zhao, J. T. Lee, G. W. Jang, X. J. Shi and J. H. Park, *J. Mater. Chem. A*, 2014, **2**, 9636.
6 B. B. Tian, J. Światowska, V. Maurice, S. Zanna, A. Seyeux, L. H. Klein and P. Marcus, *Langmuir,* 2014, **30**, 3538.
7 B. J. Li, H. Q. Cao, J. Shao and M. Z. Qu, *Chem. Commun.*, 2011, **47**, 10374.
8 N. Lavoie, P. R. L. Malenfant, F. M. Courtel, Y. Abu-Lebdeh and I. J. Davidson, *J. Power Sources*, 2012, **213**, 249.
9 D. Chen, L. H. Tang and J. H. Li, *Chem. Soc. Rev.*, 2010, **39**, 3157.
10 P. Poizot, S. Laruelle, S. Grugeon, L. Dupont and J. M. Tarascon, *Nature*, 2000, **407**, 496.
11 F. Y. Cheng, J. Liang, Z. L. Tao and J. Chen, *Adv. Mater.*, 2011, **23**, 1695.
12 F. L. Lou, H. T. Zhou, T. D. Tran, M. E. M. Buan, F. V. -Bruer, M. Rønning, J. C. Walmsley and D. Chen, *ChemSusChem*., 2014, **7**, 1335.
13 M. -S. Wu, P. -C. J. Chiang, J. -T. Lee and J. -C. Lin, *J. Phys. Chem. B*, 2005, **109**, 23279.
14 X. Chen, L. Li, X. Sun, Y. Liu, B. Luo, C. Wang, Y. Bao, H. Xu and H. Peng, *Angew. Chem. Int. Ed.,* 2011, **50**, 5486.
15 M. V. Kovalenko, M. I. Bodnarchuk, R. T. Lechner, G. Hesser, F. Schaffler and W. Heiss, *J. Am. Chem. Soc.,* 2007, **129**, 6352.
16 L. Bao, W. -L. Low, J. Jiang and J. Y. Ying, *J. Mater. Chem.*, 2012, **22**, 7117.
17 K. Pitzschel, J. M. M. Moreno, J. Escrig, O. Albrecht, K. Nielsch and J. Bachmann, *ACS Nano*., 2009, **3**, 3463.
18 S. Palchoudhury, Y. Xu, A. Rushdi, R. A. Holler and Y. Bao, *Chem. Commun.*, 2011, **48**, 10499.
19 C. Lei, F. Han, Q. Sun, W. -C. Li and A. -H. Lu, *Chem. Eur. J.*, 2014, **20**, 139.
20 Y. Yu, C. Yan, L. Gu, X. Lang, K. Tang, L. Zhang, Y. Hou, Z. Wang, M. W. Chen, O. G.Schmidt and J. Maier, *Adv. Energy Mater.,* 2013, **3**, 281.
21 M. Zhang, D. N. Lei, X. M. Yin, L. B. Chen, Q. H. Li, Y. G. Wang and T. H. Wang, *J. Mater. Chem.*, 2010, **20**, 5538.
22 G. M. Zhou, D. W. Wang, F. Li, L. L. Zhang, N. Li, Z. S. Wu, L. Wen, G. Q. Lu and H. M. Cheng, *Chem. Mater.,* 2010, **22**, 5306.
23 W. M. Zhang, X. L. Wu, J. S. Hu, Y. G. Gao and L. J. Wan, *Adv. Funct. Mater.,* 2008, **18**, 3941.
24 P. Balaya, H. Li, Kienle and J. Maier, *Adv. Funct. Mater.,* 2003, **13**, 621.
25 J. Jamnik and J. Maier, *Phys. Chem. Chem. Phys.,* 2003, **5**, 5215.
26 Y. Z. Su, S. Li, D. Q. Wu, F. Zhang, H. W. Liang, P. F. Gao, C. Cheng and X. L. Feng, *ACS Nano*, 2012, **6**, 8349.
27 Y. Xu, H. Bai, G. Lu, C. Li and G. Shi, *J. Am. Chem. Soc.,* 2008, **130**, 5856.
28 W. Wei, S. B. Yang, H. X. Zhou, I. Lieberwirth, X. L. Feng and K. Müllen, *Adv. Mater.,* 2013, **25**, 2909.
29 Z. G. Teng, G. F. Zheng, Y. Q. Dou, W. Li, C. -Y. Mou, X. H. Zhang, A. M. Asiri and D. Y. Zhao, *Angew. Chem. Int. Ed.,* 2012, **124**, 2215.
30 J. Y. Xiang, J. P. Xu, J. Zhang, J. Zhong, D. Zhang and J, P, Cheng, *Electrochem. Commun.,* 2010, **12**, 1103.
31 S. H. Yang, X. F. Song, P. Zhang, J. Sun and L. Gao, *Small,* 2014, **10**, 2270.
32 Y. L.Liu, K. L. Ai and L. H. Lu, *Chem. Rev.,* 2014, **114**, 5057.
33 C. Lei, F. Han, D. Li, W. C. Li, Q. San, X. Q. Zhang and A. H. Lu, *Nanoscale*, 2013, **5**, 1168.
34 S. Deki, Y. Aoi, J. Okibe, H. Yanagimoto, A. Kajinami and M. Mizuhata, *J. Mater. Chem.,* 1997, **7**, 1769.
35 A. Kumar and S. K. Gupta, *J. Mater. Chem. B*, 2013, **1**, 5818.
36 C. Z. Yuan, L. Yang, L. R. Hou, J. Y. Li, Y. X. Sun, X. G. Zhang, L. F. Shen, X. J. Lu, S. L. Xiong and X. W. Lou, *Adv. Funct. Mater.*, 2012, **22**, 2560.
37 D. Graf, F. Molitor, K. Ensslin, C. Stampfer, A. Jungen, C. Hierold and L. Wirtz, *Nano Lett*., 2007, **7**, 238.
38 H. Kang, A. Kulkarni, S. Stankovich, R. S. Ruoffd, S. Baika, *Carbon*, 2009, **47**, 1520.
39 Z. F. Pu, M. H. Cao, J. yang, K. L. Huang and C. W. Hu, *Nanotechnology*, 2006, **17**, 799.
40 Y. Piao, J. Kim, H. Bin Na, D. Kim, J. S. Baek, M. K. Ko, J. H. Lee, M. Shokouhimehr and T. Hyeon, *Nat. Mater.*, 2008, **7**, 242.
41 X. W. Low, C. M. Li and L. A. Archer, *Adv. Mater.*, 2009, **21**, 2536.
42 J. Wang, L. L. Li, C. L. Wong, L. F. Sun, Z. X. Shen and S. Madhavi, *RSC Adv.*, 2013, **3**, 15316.
43 R. Liu, S. M. Mahurin, C. Li, R. R. Unocic, J. C. Idrobo, H. J. Gao, S. J. Pennycook and S. Dai, *Angew, Chem. Int. Ed*., 2011, **50**, 6799.
44 X. L. Jia, Z. Chen, X. Cui, Y. T. Peng, X. L. Wang, G. Wang, F. Wei and Y. F. Lu, *ACS Nano*, 2012, **6**, 9911.
45 L. S. Shen, H. W. Song, H. Cui, X. Wen, X. L. Wei and C. X. Wang, *CrystEngComm.*, 2013, **15**, 9849.
46 X. Zhang, H. H. Liu, S. Petnikota, S. Ramakrishna and H. J. Fan, J. Mater. Chem. A, 2014, 2, 10835.
47 P. P. Lv, H. L. Zhao, Z. P. Zeng, J. Wang, T. H. Zhang and X. W. Li, J. Power Source, 2014, 259, 92.
48 T. Q. Wang, X. L. Wang, Y. Lu, Q. Q. Xiong, X. Y. Zhao, J. B. Cai, S. Huang, C. D. Gu and J. P. Tu, RSC Adv., 2014, 4, 322.
49 C. N. He, S. Wu, N. Q. Zhao, C. S. Shi, E. Z. Liu and J. J. Li, *ACS Nano*, 2012, **7**, 4459.
50 M. V. Reddy, T. Yu, C. H. Sow, X. Shen, C. T. Lim and G. V. S. Rao, *Adv. Funct. Mater.,* 2007, **17**, 2792.
51 T. Zhu, J.S. Chen and X.W. Lou, *J. Phys. Chem. C*, 2011, **115**, 9814.
52 H. J. Liu, S. H. Bo, W. J. Cui, F. Li, C. X. Wang and Y. Y. Xia, *Electrochim. Acta*, 2008, **53**, 6497.
53 J. C. Guo, Q. Liu, C. S. Wang and M. R. Zachariah, *Adv. Funct. Mater.*, 2012, **22**, 803.
54 Z. Y. Wang, D. Y. Luan, S. Madhavi, Y. Hu and X. W. Lou, *Energy Environ. Sci.*, 2012, **5**, 5252.
55 Y. Ma, B. Ding, G. Ji and J. Y. Lee, *ACS Nano*, 2013, **7**, 10870.

Graphical Abstract

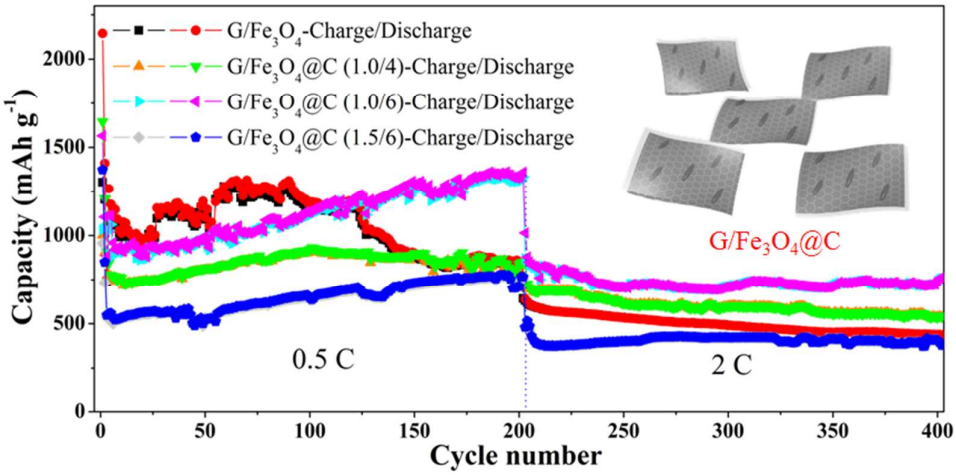

Novel hierarchical nanostructure composed of carbon coated Fe_3O_4 nanoparticles with seed-like morphology distributing on graphene ($G/Fe_3O_4@C$) is prepared as advanced anodes.